



A microfluidic microwell device operated by the automated microfluidic control system for surface-enhanced Raman scattering-based antimicrobial susceptibility testing



Cheng-Chieh Liao ^{a,1}, Yi-Zih Chen ^{b,1}, Shang-Jyun Lin ^a, Ho-Wen Cheng ^{c,d}, Juen-Kai Wang ^{c,e,f}, Yuh-Lin Wang ^c, Yin-Yi Han ^{g,h,✉*, i}, Nien-Tsu Huang ^{a,i,*}

^a Graduate Institute of Biomedical Electronics and Bioinformatics, National Taiwan University, Taipei, Taiwan

^b Department of Biomechatronics Engineering, National Taiwan University, Taipei, Taiwan

^c Institute of Atomic and Molecular Sciences, Academia Sinica, Taipei, Taiwan

^d International Graduate Program of Molecular Science and Technology, National Taiwan University (NTU-MST) and Taiwan International Graduate Program (TIGP), Academia Sinica, Taipei, Taiwan

^e Center for Condensed Matter Sciences, National Taiwan University, Taipei, Taiwan

^f Center for Atomic Initiative for New Materials, National Taiwan University, Taipei, Taiwan

^g Department of Anesthesiology, National Taiwan University Hospital, Taipei, Taiwan

^h Department of Trauma, National Taiwan University Hospital, Taipei, Taiwan

ⁱ Department of Electrical Engineering, National Taiwan University, Taipei, Taiwan

ARTICLE INFO

Keywords:

Microwell

Automated microfluidic control system

Surface-enhanced Raman scattering (SERS)

Antimicrobial susceptibility testing (AST)

ABSTRACT

Bloodstream infection (BSI) is a serious public health issue worldwide. Timely and effective antibiotics for controlling infection are crucial towards patient outcomes. However, the current culture-based methods of identifying bacteria and antimicrobial susceptibility testing (AST) remain labor-intensive and time-consuming, and are unable to provide early support to physicians in critical hours. To improve the effectiveness of early antibiotic therapy, Surface-enhanced Raman scattering (SERS) technology, has been used in bacterial detection and AST based on its high specificity and label-free features. To simplify sample preparation steps in SERS-AST, we proposed an automated microfluidic control system to integrate all required procedures into a single device. Our preliminary results demonstrated the system can achieve on-chip reagent replacement, bacteria trapping, and buffer exchange. Finally, *in-situ* SERS-AST was performed within 3.5 h by loading isolates of ampicillin susceptible and resistant *E. coli* and clear discrimination of two strains under antibiotic treatment was demonstrated. Overall, our system can standardize and simplify the SERS-AST protocol and implicate parallel bacterial detection. This prototypical integration demonstrates timely microbiological support to optimize early antibiotic therapy for fighting bacteraemia.

1. Introduction

Sepsis is a life-threatening medical emergency that is characterized by an extreme physiological response to an infection. The elicited immune and inflammatory dysregulation may further lead to organ failure. Since infection is the primary source of such seral responses, early antibiotic therapy is considered a core element to improving the chances of survival in a septic patient. Typically, the mortality rate reduces from

60% to 30% if appropriate antibiotics are given at an early stage (Ibrahim et al., 2000). To perform early and precise antibiotic therapy targeting the causative pathogen, antimicrobial susceptibility testing (AST) is the standard procedure to determine the susceptibility of bacteria to antibiotics (Abubakar et al., 2007; Ahmed et al., 2014). The current AST techniques include broth dilution tests and Kirby-Bauer disk diffusion tests (Bauer et al., 1966), as well as automated AST instruments (van Belkum et al., 2020). Although automated versions

* Corresponding author. Graduate Institute of Biomedical Electronics and Bioinformatics, National Taiwan University, Taipei, Taiwan.

** Corresponding author. Department of Anesthesiology, National Taiwan University Hospital, Taipei, Taiwan.

E-mail addresses: yyhan@ntuh.gov.tw (Y.-Y. Han), nthuang@ntu.edu.tw (N.-T. Huang).

¹ These authors made equal contributions.

greatly improved the AST operation, prolonged bacteria culture and labor-intensive sample processes are still required. Lacking timely microbiological data, physicians routinely begin empiric antibiotic therapy with either broad-spectrum antibiotics or last-line drugs and, subsequently, adjust the regimen according to the patient's clinical response or the delayed AST report. However, the efficacy of empirical therapy is unpredictable and raises the risk of clinical deterioration owing to the growing number of drug-resistant strains, which are further favored through the use of broad-spectrum antibiotics. Given the difficult situation of culture-based methods, nucleic acid amplification technologies (NAATs) (Sinha et al., 2018) and matrix-assisted laser desorption ionization-time of flight mass spectroscopy (MALDI-TOF MS) (Oviano and Bou, 2018) are developed to identify drug-resistant bacteria that are non-cultivable or in low concentrations. However, interference from co-existing human DNA fragments, protein constituents or ineffective lysis of bacteria may impair diagnosis.

Microfluidic technology has been developed to perform AST as it bears three advantages. First, bacteria are better contained in the microenvironment for parallel AST (Choi et al., 2013; Matsumoto et al., 2016). Second, confinement in the microenvironment enables precise cell counting and identification (Jalali et al., 2017; Takagi et al., 2013). With an extremely small trapping region, single-bacterium AST is even achievable via microfluidics (Choi et al., 2014; Li et al., 2019). Third, microfluidics can apply various external fields to enrich or stimulate bacteria, thus improving the quality of AST. One example is integrating dielectrophoresis (DEP) with microfluidics to purify bacteria from blood (Yi et al., 2019). Another example is using microfluidics to create a high-stress environment to accelerate bacterial responses to antibiotics (Kalashnikov et al., 2017). Generally, these systems take images of bacteria using high-resolution imaging setups and image processing programs; bacteria accumulation or uneven distribution may, however, affect the accuracy. Other methods, preventing above-mentioned issues, measure the characteristics of bacteria or the surrounding medium during antibiotic treatment, including the medium pH value (Cira et al., 2012; Lee et al., 2017), electrical conductivity (Onishi et al., 2018), bacterial impedance (Safavieh et al., 2017), and bacterial secreted metabolites (Liu et al., 2016).

Surface-enhanced Raman scattering (SERS) is another technique that has been implemented into microorganism analysis owing to its label-free, highly specific, and accurate sensing features. SERS is an optical detection technique that can greatly enhance the Raman scattering signal of molecules attached to metallic nanostructures or nanoparticles due to surface plasmon resonance (electromagnetic enhancement) and/or intermolecular/intramolecular charge transfer (chemical enhancement). Recently, SERS-based bacteria identification, functional analysis of microorganisms, complex biofilm characterization, and AST have been explored (Cui et al., 2019; Wang et al., 2018). Research showed that ribosomal degradation occurs in bacteria in nutrition-insufficient environments (Ben-Hamida and Schlessinger, 1966; Kaplan and Apirion, 1975; Maruyama and Mizuno, 1970), which results in the secretion of purine metabolites (Link et al., 2015), including adenine, hypoxanthine, xanthine, guanine, uric acid, and adenosine monophosphate. These purine derivatives provide characteristic SERS signals of bacteria for their identification or metabolism monitoring (Liu et al., 2016; Premasiri et al., 2016). Compared to conventional optical density (OD)-based AST methods with overnight incubation, SERS-based AST requires only ~2–3 h incubation followed by another ~1–2 h for processing and detection. Furthermore, the label-free sensing feature allows SERS measurements to be easily integrated with microfluidics for bacteria enrichment or encapsulation. For example, filter membranes (Chang et al., 2019) and microwells (Huang et al., 2020) have been integrated with the SERS substrate for *in-situ* SERS-AST. Although the integration showed some advantages, multiple sample preparation processes still need to be performed off-chip, meaning the whole SERS-AST process remained labor-intensive and time-consuming.

Here, we proposed an automated microfluidic control system to fully

integrate all SERS-AST procedures, including antibiotic treatment, bacteria culture, isolation, and *in-situ* SERS measurement, into one single chip. Since all reagent flows are controlled by the automated microfluidic control system, the microfluidic device can be easily fabricated in a single-layer format without complicated microvalve alignment or tube connection and attached to the SERS substrate. A key point regarding on-chip bacteria culture and antibiotic treatment is to ensure that the bacteria are well-contained in the microwell during the buffer washing process. The washing process serves two purposes: first, it can minimize the SERS signal interference from the culture medium and, second, the nutrient-insufficient environment can further stimulate bacteria to secrete more metabolites. For proof of concept, we loaded two *E. coli* strains to rehydrated vacuum-dried antibiotics and performed on-chip bacteria culture and antibiotic treatment. Finally, the microwells containing isolated bacteria was attached to the SERS substrate for *in-situ* SERS-AST measurement. Based on the above features, we envision a rapid, sample-efficient, and fully integrated SERS-AST platform, which can help physicians to monitor patients' conditions and optimize timely treatments.

2. Materials and methods

2.1. Bacterial samples

Escherichia coli (*E. coli*, BW25113) that served as the AMP (ampicillin) susceptible strain, was received from Shared Information of Genetic Resources, SHIGEN, supported by the National Bioresource Project. *E. coli* (DH5 α) purchased from Eastern Biotech Co., Ltd., was transformed with a pGS-21 plasmid for AMP resistance and served as the resistant strain. AMP was purchased from Sigma-Aldrich. To prepare bacteria samples, a small number of cells were picked up from individual colonies on an agar plate using an inoculation loop and then suspended in a culture tube with 5 mL Mueller Hinton Broth (MHB, BD BBL). The tube was then placed in an incubator on a shaker at 200 rpm and cultured overnight (~12–18 h) at 37 °C. Next, a 200 μ L sample from overnight culture was added to 5 mL fresh medium and sub-cultured for 3 h until the optical density of the samples at 600 nm (OD₆₀₀) reached 0.5 — around 10⁸ CFU/mL. The sub-cultured sample was diluted or centrifuged to the target concentration.

2.2. The microfluidic microwell device and SERS substrate fabrication

The microfluidic microwell device is composed of a microchannel layer and a microwell layer. Both layers are made of polydimethylsiloxane (PDMS, Sylgard-184, Dow Corning) based on the standard soft lithography process (Huang et al., 2018). Here, the microwell was temporarily bonded with the microchannel layer by the electrostatic force, which can be detached and bonded to the SERS substrate. The SERS substrate was fabricated following our previous protocol (Chang et al., 2019). Briefly, the glass slide was first pre-cleaned by acetone and hydrofluoric acid and then the silver-island film was deposited by the E-beam evaporator (EBS-300, Junsun Tech) at 0.3 nm/min evaporation rate with an average thickness of 7 nm.

2.3. SERS measurement and spectral processing

The SERS spectra were captured by the Raman system constructed by a standard epi-fluorescent microscope (BX61WI, Olympus) equipped with a Raman fiber probe (SuperHead HE 640, Horiba Jobin Yvon) and a spectrometer (HE 633, Horiba) attaching a thermoelectric-cooled charge-coupled device (CCD) (354308, Horiba). The light source, 5 mW 632.8 nm HeNe laser (LGK 7665 P18, LASOS), was first filtered by a band-pass filter and focused on the SERS substrate. The scattered light was obtained with a 0.5 s integration time by a 20 \times objective lens (MPlanFL N, Olympus, laser spot size: ~25 μ m), for spectral measurement. The spectral resolution and error were 4 and 0.1 cm⁻¹,

respectively. The spectral resolution is based on the available pixel numbers of CCD and the spectral error is caused by the spectral distortion of scattering light with a curve surface projected on the flat CCD array. For multiple microwell measurements, the device was raster-scanned by a motorized stage (EK32 75x50, Märzhäuser). Each SERS spectrum was averaged over 3 repeat cycle and then processed under the baseline removal program based on the nonlinear iterative peak clipping algorithm (Morháč and Matoušek, 2008). Here, we use the intensity of 733 cm^{-1} Raman shift (I_{733}) as the main parameter to represent the amount of bacteria-secreted purine derivatives. To calculate the I_{733} value, we first found the maximum peak intensity within the $733 \pm 20\text{ cm}^{-1}$ range and then integrated the intensity in the $\pm 40\text{ cm}^{-1}$ range.

2.4. Bright-field and fluorescent optical imaging setup

The bright-field and fluorescent videos or images were captured by an inverted fluorescence microscope (IX-73, Olympus) equipped with a dual-color charge-coupled device (CCD) camera (DP-80, Olympus) using 2X, 4X, 10X, 20X, and 40 \times (PlanN, Olympus) objectives. Stitching images were composed using the supplied microscopic analysis software (CellSens, Olympus). ImageJ software was used to quantify bacterial numbers in the microwells and calculate fluorescent intensities.

2.5. The automated microfluidic control system and microfluidic microwell device design

The schematic of the automated microfluidic control system is shown in Fig. 1A. Briefly, the system was built up by the uProcess interface (EIB200, LabSmith). First, DI water and air are preloaded into two reservoirs (BBRES-1ML, LabSmith) and drawn by an 80 μL syringe pump

(SPS01-080-C360, LabSmith) for buffer replacement and air isolation, respectively. The liquid and air flow directions are switched and guided by two automated selector valves (3-port, AV201-C306 LabSmith) connected by 150 μm capillary tubes (CAP360-150P, LabSmith). The pump and valves, including the flow rate, direction, and period, are controlled by the customized program (uProcess 1.46). Fig. 1B illustrates a photo of the automated microfluidic control system. A photo of the microfluidic microwell device under the air isolation process is shown in Fig. 1C. The olive shape design can eliminate potential bubble issues during the air isolation process. Here, the DI water was mixed with blue food dye for clear observation. The red-framed inset shows the air-liquid interface during the air isolation process. The yellow-framed inset contains a magnified image of the 12 \times 12 air-isolated microwells, indicating that the DI water is confined to the microwell without leakage. The diameter and depth of a single microwell are both 50 μm and the density is 100 microwells per mm². The microchannel attached on the top of the microwell layer can cover over 2000 microwells.

3. Results and discussion

3.1. The SERS-AST protocol

The SERS-AST protocol operated by the automated microfluidic control system is shown in Fig. 2. In brief, the process can be divided into seven steps comprising four parts. The first part is “antibiotic preloading,” which includes antibiotic injection, isolation, and vacuum drying. The process allows antibiotic storage in advance and simplifies the following bacterial loading step. To achieve this feature, the antibiotic solution was first injected at pre-calculated concentrations in order to fill the entire microfluidic device (step 1). Next, the antibiotic solution was

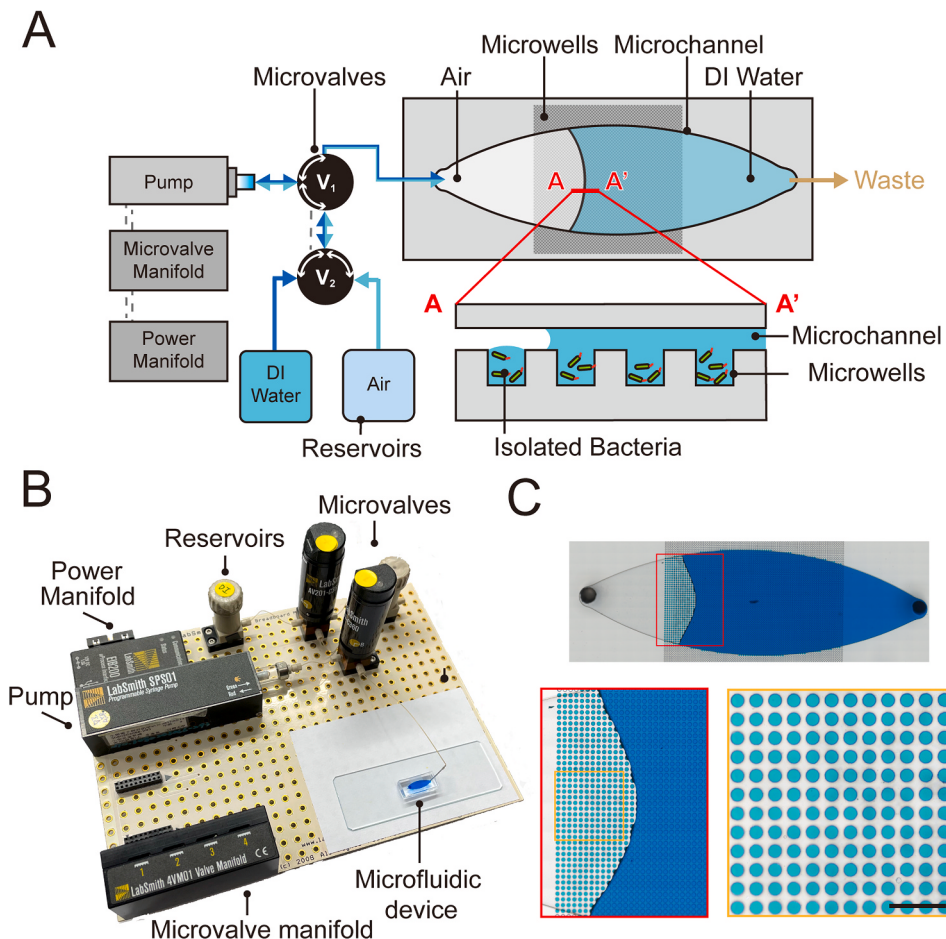


Fig. 1. (A) Schematic and (B) photograph of the microfluidic microwell device operated by the automated microfluidic control system, consisting of one syringe pump, two microvalves, two reservoirs, and one microvalve manifold. The dimensions of the whole system and the microfluidic microwell device are 18.5 cm \times 13.3 cm and 15 mm \times 3.6 mm, respectively; (C) photo of the microfluidic microwell device under the air isolation process. DI water was mixed with blue food dye for clear observation. The red-framed inset shows the air-liquid interface during the air isolation process. The yellow-framed inset highlights a magnified image showing 12 \times 12 air-isolated microwells. Scale bar: 200 μm . (For interpretation of the references to color in this figure legend, the reader is referred to the Web version of this article.)

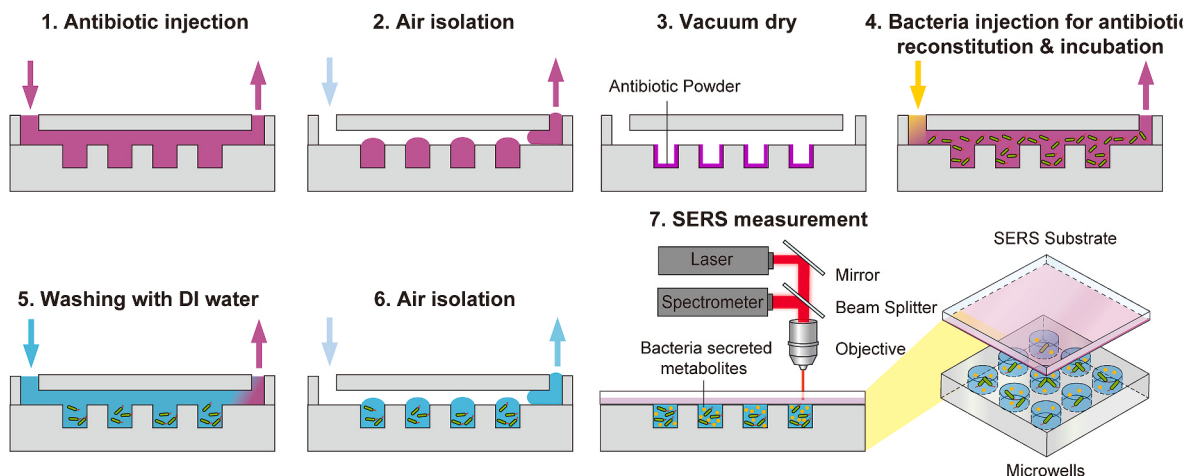


Fig. 2. The SERS-AST protocol operated by the automated microfluidic control system. The protocol can be divided into four parts comprising seven steps: (1) “antibiotic preloading”, including antibiotic injection, isolation, and drying (steps 1–3); (2) “bacteria injection for antibiotic reconstitution and incubation” (step 4); (3) “DI water washing and air isolation” (steps 5–6); and (4) SERS substrate attachment for multiparallel *in-situ* “SERS measurement” (step 7).

flushed with air and isolated in the microwells (step 2). Then, the antibiotic solution was vacuum-dried to form a powder in the microwells (step 3); this step makes the following reconstitution more uniform, since the antibiotic can be evenly rehydrated from each microwell and distributed to the whole device. The second part is “bacteria injection for antibiotic reconstitution and incubation”. Once the bacterial sample was introduced into the device, the vacuum-dried antibiotics could be reconstituted to immediately treat the sample. Here, the bacterial samples were incubated with antibiotics for 3 h (step 4). The third part is “DI water washing and air isolation”. DI water was flushed through the device to replace the bacteria culture medium while the bacteria were contained within the microwells (step 5). Next, air was introduced into the device to isolate each microwell (step 6). The last part is “SERS measurement”. The top microchannel layer was gently lifted by hand and the bottom microwell layer filled with liquid was covered by the SERS substrate to perform *in-situ* SERS measurement (step 7). As the SERS measurement is performed at the interface of the SERS substrate and the top surface of the microwell, it mitigates potential bacterial attachment on the SERS substrate and, thus, ensures that the SERS signal is mainly contributed by secreted metabolites in the surrounding solution. Operated by the automated microfluidic control system, all reagent flow parameters, including (1) flow rate; (2) flow volume; (3) flow direction; and (4) pause time, are fully programmable, thus eliminating labor-intensive operations and potential human error.

3.2. Reagent reconstitution

To realize “antibiotic preloading” process, we needed to confirm that antibiotics were injected, vacuum dried and be uniformly rehydrated in the individual microwells following subsequent liquid injection. If the reagent remains only in the microwells and dehydrates, the ratio of the subsequently reconstituted concentration to the original concentration is equivalent to the volume ratio of the microwell to the whole device (microchannel + microwell), approximately 8%. To evaluate the performance of reagent reconstitution, we used the Fluorescein isothiocyanate (FITC) solution to mimic the antibiotics to facilitate concentration calculations based on the fluorescent intensity. Detailed FITC reconstitution process is shown in supplemental information. As shown in Fig. S1A, the fluorescent intensity of the reconstituted FITC was correlated to the equivalent concentration of ~0.949–0.982 µg/mL (Fig. S1B), which is similar to the theoretical value (8% of original solution at 10 µg/mL), confirming the validity of the reconstitution process.

3.3. Buffer washing flow rate optimization

Next, we evaluated the bacteria encapsulation result in “bacteria injection for antibiotic reconstitution and incubation” process. First, we optimize the washing flow rate, which can replace culture medium while still keeping most bacteria encapsulated in the microwells. To mimic the bacteria, we infused 2.0 µm fluorescent beads (Fluoresbrite® Polychromatic Red Microspheres, Polysciences), at a concentration of 5×10^7 /mL, into the device for 3 h sedimentation. Then, we flowed DI water at 5, 10, and 20 µL/min for 3 min to replace the remaining solution and beads that were not inside a microwell. To calculate the number of encapsulated beads in a microwell, we selected a total of 1100 microwells (grid of 55 rows and 20 columns) at the center of the microchannel and captured the corresponding fluorescence images, as shown in Fig. 3A. The insets show magnified images of 9 microwells containing beads. To quantify the bead number and distribution profile, we used the imaging processing algorithm to transfer the fluorescent intensity. The detailed image processing protocol is shown in supplemental information. The intensity transformed bead heat maps and bead distribution profiles at various washing flow rates are shown in Fig. 3B and C, respectively. Results demonstrated that the average bead number inside a microwell is 37 prior to the washing step. After 5 and 10 µL/min flow rates, the average bead numbers were 36 counts per microwell, almost identical to the beads number before washing. In contrast, the bead number dropped to 24 counts per microwell at 20 µL/min flow rate. To sum up, both 5 and 10 µL/min flow rates could confine most beads to the microwells. Based on this experiment, we selected 10 µL/min as the washing flow rate for subsequent experiments.

3.4. SERS measurement for bacteria encapsulated in microwells

Next, we evaluated the buffer exchange effect in “DI water washing and air isolation” process under the optimized washing conditions. To analyze the effects of the surrounding buffer on the SERS signal, we injected 10^8 CFU/mL susceptible *E. coli* cultured in pure MHB medium into the microfluidic microwell device without any buffer washing step and then measured the SERS spectrum (blue line in Fig. 4A). For comparison, two additional bacteria samples were either (1) subjected to the off-chip manual centrifugation-purification process and then loaded into the device (orange line in Fig. 4A) or (2) directly loaded into the device and then subjected to the automated buffer washing process (red line in Fig. 4A). As a reference, pure MHB medium was injected into the device using the automated buffer washing process (gray line in Fig. 4A). All four samples were then air-isolated in the microwells for subsequent

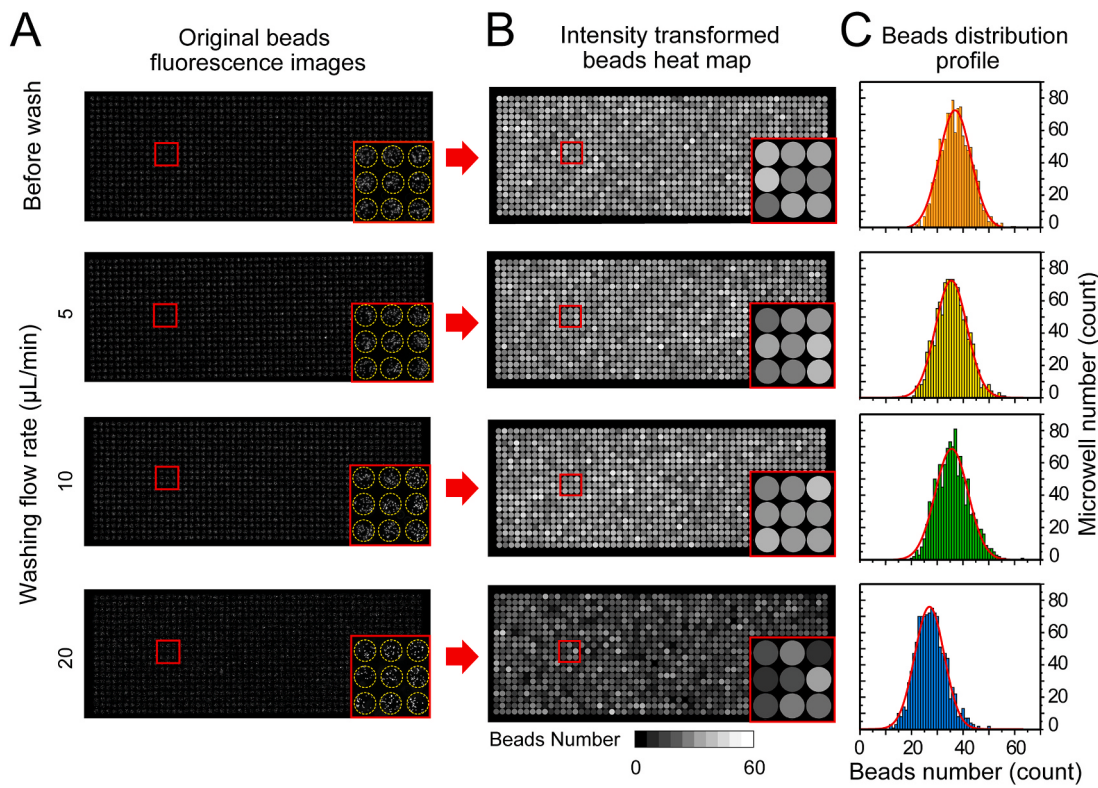


Fig. 3. Washing flow rate optimization. (A) Fluorescence images of microwell array encapsulated beads before and after the DI washing process at 5, 10, 20 $\mu\text{L}/\text{min}$; (B) the intensity transformed bead seeding profiles; (C) the beads distribution profiles among 1100 microwells. The four distribution profiles all showed a normal distribution profile. Both 5 and 10 $\mu\text{L}/\text{min}$ washing rates resulted in similar distribution profiles when compared to the before washing case (p -value > 0.05).

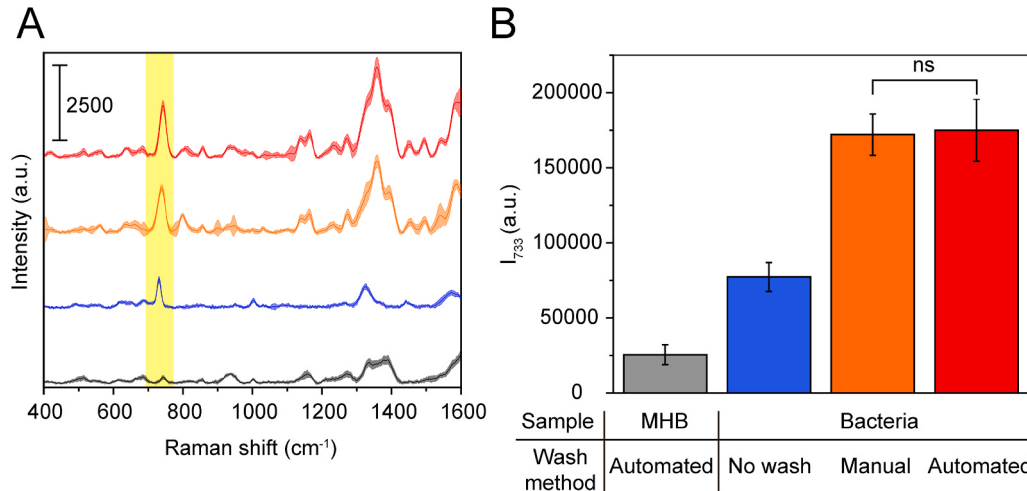


Fig. 4. Comparison of DI water washing protocols. (A) SERS spectra of pure MHB (black line), bacteria without washing process (blue line), bacteria under manual centrifugation-purification process (orange line), and bacteria under automated DI water washing process (red line). The light bands represent the corresponding standard deviations. (B) Comparison of the 733 cm^{-1} Raman intensities (I_{733}) of the four samples. After the DI water washing process, all samples were injected into the microfluidic microwell device followed by the air isolation process for multiparallel *in-situ* SERS measurement. (ns: statistically not significant). (For interpretation of the references to color in this figure legend, the reader is referred to the Web version of this article.)

“SERS measurement” process. The SERS spectra and I_{733} of four samples are shown in Fig. 4A and B, respectively. Here, three qualitative results can be summarized. First, when comparing the I_{733} of pure MHB (gray bar in Fig. 4B) to the bacteria sample (red bar in Fig. 4B) subjected to the automated washing process, a significantly stronger I_{733} signal is seen in the bacterial case, indicating that the SERS signal in the microwells mainly represents metabolites secreted from bacteria. Second, by comparing the I_{733} of bacteria samples with and without (blue bar) application of the washing process, we found that both off-chip (orange bar) and on-chip (red bar) buffer washing processes enhanced the metabolite secretion from bacteria, based on higher I_{733} levels, confirming that bacteria secrete more metabolites in a nutrition-insufficient

environment. Additionally, signals of both washing methods were statistically insignificant, indicating that the automated washing process offers a more compact and easier buffer exchange protocol with similar performance.

3.5. Antimicrobial susceptibility testing using the automated microfluidic control system

Finally, we demonstrate *in-situ* SERS-AST using the automated microfluidic control system. The ability to quantify the SERS signals of secreted bacterial metabolites at various concentrations of bacteria is an essential requirement for SERS-AST. For proof of concept, susceptible

E. coli were adjusted to $\sim 10^7\text{--}10^{10}$ CFU/mL and manually washed via the off-chip centrifugation. Next, the purified bacterial samples were loaded into the microfluidic microwell device following the SERS-AST protocol. The SERS spectra and I_{733} signals of all bacterial samples are shown in Fig. 5A and B, respectively. We discovered that the SERS signal increased with increasing bacterial concentrations, with all values significantly higher than pure MHB. To counter potential increases in bacterial concentration during the 3 h incubation period with antibiotics in the microfluidic device, we designated 5×10^7 CFU/mL as the initial concentration for *in-situ* SERS-AST. Next, we injected susceptible and resistant *E. coli* strains into individual devices for a 3 h incubation to reconstitute antibiotic solutions of dried AMP at concentrations of 0, 4, 8, 16, 32 $\mu\text{g}/\text{mL}$. Following the incubation, the buffer washing and bacteria isolation processes were performed by the automated microfluidic control system.

The SERS spectra of susceptible and resistant *E. coli* treated with various concentrations of AMP are shown in Fig. 6A and B, respectively. For susceptible strains, a clear drop of I_{733} was observed at 32 $\mu\text{g}/\text{mL}$ of AMP (Fig. 6C), indicating growth suppression of bacteria by AMP at this concentration. In contrast, I_{733} values remained relatively unchanged across all AMP concentrations for resistant strains (Fig. 6D). To further quantify the signal difference between the two strains and determine the susceptibility, we utilized the parameter r_{733} , which represents the I_{733} ratio of bacteria with and without antibiotic treatment ($r_{733} = \frac{I_{733, \text{treated}}}{I_{733, \text{not treated}}}$). The standard deviation of r_{733} is defined as the propagation

of error: $\delta(r_{733}) = r_{733} \times \sqrt{\left(\frac{\delta(I_{733, \text{treated}})}{I_{733, \text{treated}}}\right)^2 + \left(\frac{\delta(I_{733, \text{not treated}})}{I_{733, \text{not treated}}}\right)^2}$. As shown in Fig. 6E, r_{733} of the susceptible *E. coli* under 4 and 8 $\mu\text{g}/\text{mL}$ AMP treatment is higher than 1.0. The ratio started to decrease at 16 $\mu\text{g}/\text{mL}$ AMP and dropped to 0.22 at 32 $\mu\text{g}/\text{mL}$ AMP. In contrast, the r_{733} values of the resistant *E. coli* strains were $\sim 0.74\text{--}0.84$ across all four AMP concentrations. The distinct SERS pattern demonstrate that two strains can successfully be discriminated by our system.

Based on the results, the SERS signal of susceptible strains at low concentrations of AMP (i.e., 4 and 8 $\mu\text{g}/\text{mL}$) was even higher than that of the samples without AMP treatment. We suspect this is due to the hormetic effect, a biphasic dose-response phenomenon characterized by low-dose stimulation and high-dose inhibition (Davies et al., 2006; Mathieu et al., 2016; Migliore et al., 2013). At sub-inhibitory or non-lethal concentrations, complex adaptive cellular responses, such as extracellular secretion of purine metabolites or DNA release related to antibiotic tolerance may be induced giving the elevated SERS signal (Bernier and Surette, 2013; Das and Manfield, 2012; Kaplan et al., 2012). For comparison, an AST using the standard broth dilution method was conducted (Fig. S2A). Following the guidance of the

Clinical & Laboratory Standards Institute (CLSI), 5×10^5 CFU/mL of both susceptible and resistant strains were treated with AMP at various concentrations (0–256 $\mu\text{g}/\text{mL}$) and then incubated overnight at 37 °C. Referencing the OD₆₀₀ value calculated at each antibiotic concentration (Fig. S2B), 16 $\mu\text{g}/\text{mL}$ (red circle) was determined as the MIC of AMP for the susceptible strain, whereas the OD₆₀₀ value remained constant in the resistant strain, even at the highest drug concentration. In contrast to the biphasic response shown in the SERS-AST results, the OD₆₀₀ values of susceptible strain decreased gradually as the drug concentrations increased, without any paradoxical rise at lower drug concentrations, e.g., 4 and 8 $\mu\text{g}/\text{mL}$. Although OD measurement is widely used to estimate biomass in microbial processes based on its rapid, low cost, and non-destructive features, the correlation may need to be calibrated under several circumstances, such as particulates existing in the medium, bacteria aggregation or low bacteria concentration. Especially for AST application, bacteria elongation effect under antibiotic-induced filamentation (Stevenson et al., 2016) may affect its accuracy. Furthermore, OD measurement required prolonged culture time, which cannot provide timely information for clinical decision making. Comparatively, SERS technique measures the metabolites secreted by bacteria, reflecting its vitality, and would not be affected by bacteria aggregation or elongation effect. Therefore, SERS technique seems to be a more rapid and sensitive tool to monitor bacterial response to antibiotic treatment by the alteration on metabolism. However, further studies on the detailed mechanisms by which SERS signals increase at low AMP doses are still required to draw a solid conclusion.

4. Conclusions

We demonstrated a microfluidic microwell device operated by the automated microfluidic control system to perform *in-situ* SERS-AST. Overall, three important features were demonstrated. First, the antibiotic can be preloaded and vacuum-dried in the microfluidic device, enabling on-chip bacterial stimulation by simply loading bacterial samples. Second, the microfluidic control system can perform the automatic buffer washing process to eliminate the SERS interference from the medium while retaining the majority of bacteria in the microwells. Besides, the buffer washing process is gentler, preventing bacteria from suffering high-pressure or shear-stress environments, and can simultaneously process thousands of bacteria-encapsulated microwells. Third, the *in-situ* SERS measurement in the microwells can realize a high-throughput AST with minimum sample requirement. The entire processing time from bacterial injection to final SERS measurement consumes only 3.5 h, much faster than previous SERS-AST methods. The limitation of the current setup is the relatively low spectra measurement

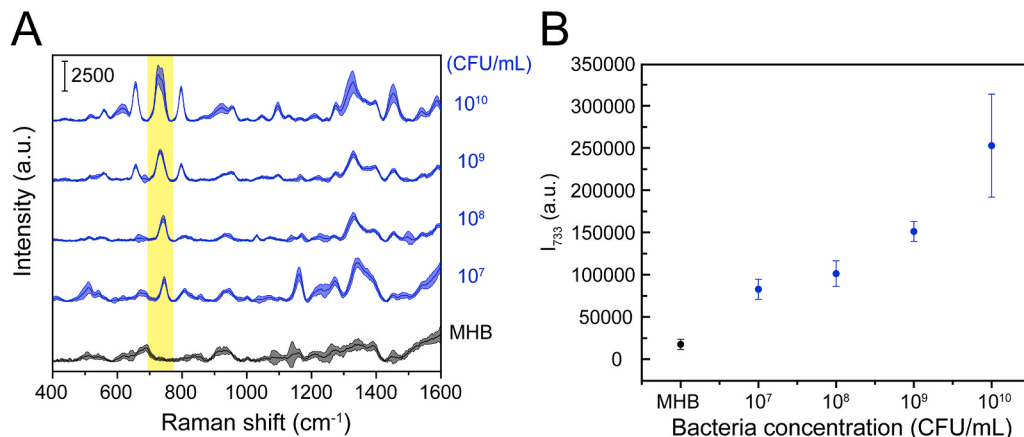


Fig. 5. (A) SERS spectra of secreted metabolites of susceptible *E. coli* at $\sim 10^7\text{--}10^{10}$ CFU/mL. The light bands represent the corresponding standard deviations. (B) I_{733} (highlighted with yellow in the SERS spectra) plotted as a function of the bacteria concentration in (A). (For interpretation of the references to color in this figure legend, the reader is referred to the Web version of this article.)

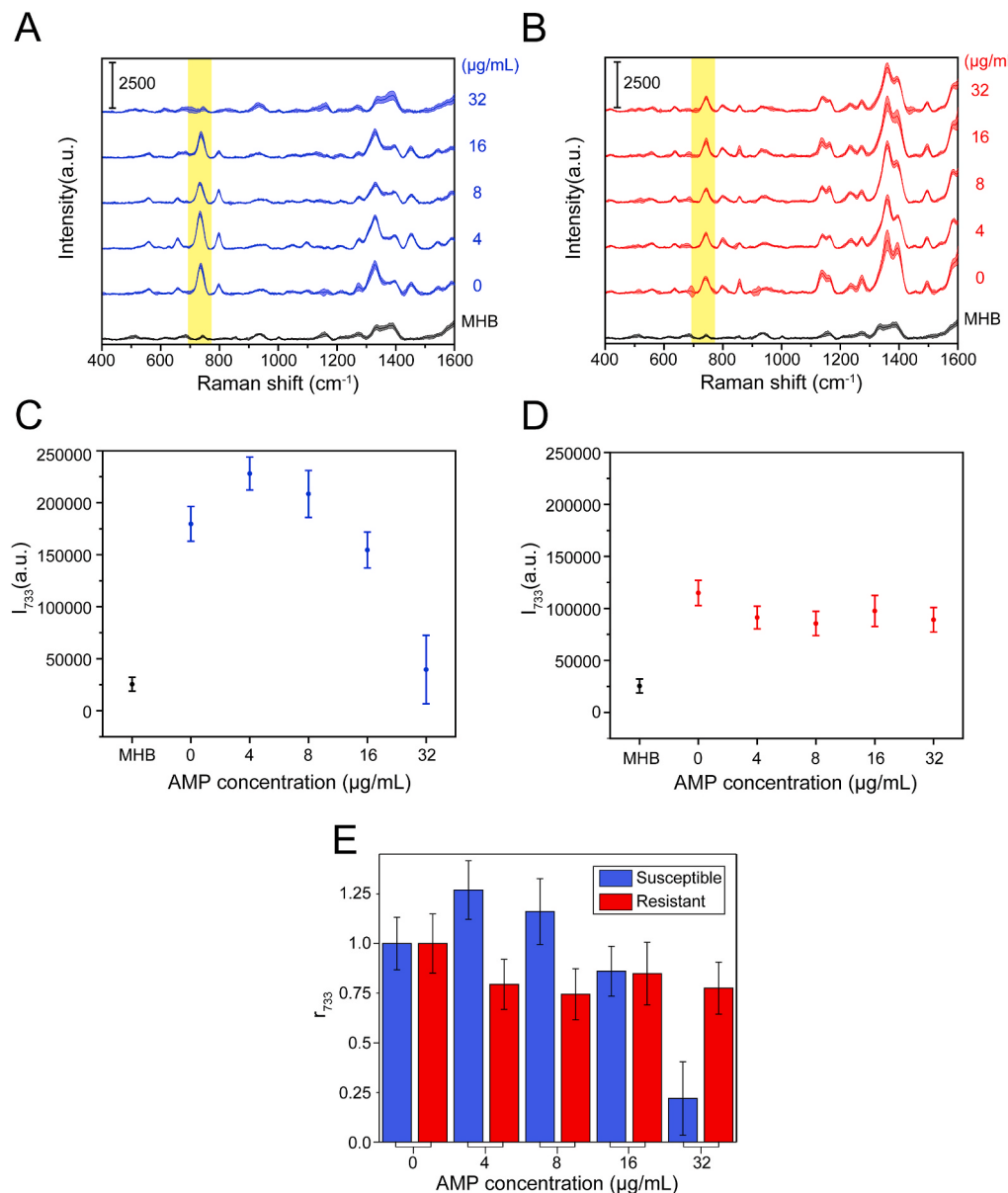


Fig. 6. AST results of AMP-susceptible and -resistant *E. coli* treated with AMP for 3 h in the automated microfluidic control system: SERS spectra of (A) the susceptible and (B) the resistant strain treated with AMP at concentrations of 0, 4, 8, 16, or 32 µg/mL. The black line represents the SERS spectrum of MHB as a reference. The light bands represent the corresponding standard deviations. (C and D) The 733 cm^{-1} Raman intensities of (C) the susceptible strain and (D) the resistant strain treated with AMP at a concentration of 0, 4, 8, 16, or 32 µg/mL. (E) The ratio of the signal strength at 733 cm^{-1} (r_{733}) of the susceptible and resistant strains following treatment with AMP at a concentration of 0, 4, 8, 16, or 32 µg/mL.

throughput, which can be improved by integrating the control program of the motorized stage with spectral measurement. Another direction for improvement is to increase bacterial distribution uniformity by optimizing the microwells dimensions or design a microfluidic concentration gradient generator (Kim et al. 2015, 2019) to load antibiotics of various concentrations for multiplex AST. Based on the above features, we envision the system can provide physicians timely AST results to support and optimize early antibiotic therapy when fighting bacteremia.

Author contributions

C.-C. Liao designed and performed experiments, data analysis, and prepared the manuscript; Y.-Z. Chen and S.-J. Lin conducted bacteria culture, data analysis and revised the manuscript; H.-W. Cheng provided the SERS substrate and assisted with Raman measurement; Y.-Y. Han assisted in data analysis and wrote the manuscript; J.-K. Wang and Y.-L. Wang provided suggestions of experiments and the interpretation of data; N.-T. Huang proposed the original idea, guided experiments, and wrote the manuscript.

Declaration of competing interest

The authors declare that they have no known competing financial interests or personal relationships that could have appeared to influence the work reported in this paper.

Acknowledgment

This work was supported by the Ministry of Science and Technology, Taiwan under the grant "MOST 109-2221-E-002-044" and "MOST 109-2639-M-001-005-ASP", and National Taiwan University Hospital under the grant "UN109-061". We are thankful to Dr. Jun-Yi Chien for providing AMP-resistance transfected *E. coli*.

Appendix A. Supplementary data

Supplementary data to this article can be found online at <https://doi.org/10.1016/j.bios.2021.113483>.

References

- Abubakar, I., Irvine, L., Aldus, C.F., Wyatt, G.M., Fordham, R., Schelenz, S., Shepstone, L., Howe, A., Peck, M., Hunter, P.R., 2007. *Health Technol. Assess.* 11 (36), 1–216.
- Ahmed, A., Rushworth, J.V., Hirst, N.A., Millner, P.A., 2014. *Clin. Microbiol. Rev.* 27 (3), 631–646.
- Bauer, A.W., Kirby, W.M.M., Sherris, J.C., Turck, M., 1966. *Am. J. Clin. Pathol.* 45 (4), 493–496.
- Ben-Hamida, F., Schlessinger, D., 1966. *Biochim. Biophys. Acta Nucleic Acids Protein Synth.* 119 (1), 183–191.
- Bernier, S., Surette, M., 2013. *Front. Microbiol.* 4 (20).
- Chang, K.-W., Cheng, H.-W., Shiue, J., Wang, J.-K., Wang, Y.-L., Huang, N.-T., 2019. *Anal. Chem.* 91 (17), 10988–10995.
- Choi, J., Jung, Y.-G., Kim, J., Kim, S., Jung, Y., Na, H., Kwon, S., 2013. *Lab Chip* 13 (2), 280–287.
- Choi, J., Yoo, J., Lee, M., Kim, E.-G., Lee, J.S., Lee, S., Joo, S., Song, S.H., Kim, E.-C., Lee, J.C., Kim, H.C., Jung, Y.-G., Kwon, S., 2014. *Sci. Transl. Med.* 6 (267), 267ra174.
- Cira, N.J., Ho, J.Y., Dueck, M.E., Weibel, D.B., 2012. *Lab Chip* 12 (6), 1052–1059.
- Cui, L., Zhang, D., Yang, K., Zhang, X., Zhu, Y.-G., 2019. *Anal. Chem.* 91 (24), 15345–15354.
- Das, T., Manefield, M., 2012. *PLoS One* 7 (10), e46718.
- Davies, J., Spiegelman, G.B., Yim, G., 2006. *Curr. Opin. Microbiol.* 9 (5), 445–453.
- Huang, H.-K., Cheng, H.-W., Liao, C.-C., Lin, S.-J., Chen, Y.-Z., Wang, J.-K., Wang, Y.-L., Huang, N.-T., 2020. *Lab Chip* 20 (14), 2520–2528.
- Huang, N.-T., Hwong, Y.-J., Lai, R.L., 2018. *Microfluid. Nanofluidics* 22 (2), 16.
- Ibrahim, E.H., Sherman, G., Ward, S., Fraser, V.J., Kollef, M.H., 2000. *Chest* 118 (1), 146–155.
- Jalali, F., Ellett, F., Irimia, D., 2017. *Technology* 5 (2), 107–114.
- Kalashnikov, M., Mueller, M., McBeth, C., Lee, J.C., Campbell, J., Sharon, A., Sauer-Budge, A.F., 2017. *Sci. Rep.* 7 (1), 8031.
- Kaplan, J.B., Izano, E.A., Gopal, P., Karwacki, M.T., Kim, S., Bose, J.L., Bayles, K.W., Horswill, A.R., 2012. *mBio* 3 (4), e00198.
- Kaplan, R., Apirion, D., 1975. *J. Biol. Chem.* 250 (5), 1854–1863.
- Kim, S., Masum, F., Kim, J.-K., Chung, H.J., Jeon, J.S., 2019. *Lab Chip* 19 (6), 959–973.
- Kim, S.C., Cestellos-Blanco, S., Inoue, K., Zare, R.N., 2015. *Antibiotics* 4 (4), 455–466.
- Lee, W.-B., Fu, C.-Y., Chang, W.-H., You, H.-L., Wang, C.-H., Lee, M.S., Lee, G.-B., 2017. *Biosens. Bioelectron.* 87, 669–678.
- Li, H., Torab, P., Mach, K.E., Surette, C., England, M.R., Craft, D.W., Thomas, N.J., Liao, J.C., Puleo, C., Wong, P.K., 2019. *Proc. Natl. Acad. Sci. U.S.A.* 116 (21), 10270.
- Link, H., Fuhrer, T., Gerosa, L., Zamboni, N., Sauer, U., 2015. *Nat. Methods* 12 (11), 1091–1097.
- Liu, C.Y., Han, Y.Y., Shih, P.H., Lian, W.N., Wang, H.H., Lin, C.H., Hsueh, P.R., Wang, J. K., Wang, Y.L., 2016. *Sci. Rep.* 6, 23375.
- Maryama, H., Mizuno, D.i., 1970. *Biochim. Biophys. Acta Nucleic Acids Protein Synth.* 199 (1), 159–165.
- Mathieu, A., Fleurier, S., Frénoy, A., Dairou, J., Bredeche, M.-F., Sanchez-Vizcute, P., Song, X., Matic, I., 2016. *Cell Rep.* 17 (1), 46–57.
- Matsumoto, Y., Sakakihara, S., Grushnikov, A., Kikuchi, K., Noji, H., Yamaguchi, A., Iino, R., Yagi, Y., Nishino, K., 2016. *PLoS One* 11 (2), e0148797.
- Migliore, L., Rotini, A., Thaller, M.C., 2013. *Dose-Response* 11(4), dose-response. Migliore, pp. 13–1002.
- Morháč, M., Matousek, V., 2008. *Appl. Spectrosc.* 62 (1), 91–106.
- Onishi, K., Enomoto, J., Araki, T., Takagi, R., Suzuki, H., Fukuda, J., 2018. *Analyst* 143 (2), 396–399.
- Oviano, M., Bou, G., 2018. *Clin. Microbiol. Rev.* 32 (1) e00037-00018.
- Premasiri, W.R., Lee, J.C., Sauer-Budge, A., Théberge, R., Costello, C.E., Ziegler, L.D., 2016. *Anal. Bioanal. Chem.* 408 (17), 4631–4647.
- Safavieh, M., Pandya, H.J., Venkataraman, M., Thirumalaraju, P., Kanakasabapathy, M. K., Singh, A., Prabhakar, D., Chug, M.K., Shafiee, H., 2017. *ACS Appl. Mater. Interfaces* 9 (14), 12832–12840.
- Sinha, M., Jupe, J., Mack, H., Coleman, T.P., Lawrence, S.M., Fraley, S.I., 2018. *Clin. Microbiol. Rev.* 31 (2) e00089-00017.
- Stevenson, K., McVey, A.F., Clark, I.B.N., Swain, P.S., Pilizota, T., 2016. *Sci. Rep.* 6 (1), 38828.
- Takagi, R., Fukuda, J., Nagata, K., Yawata, Y., Nomura, N., Suzuki, H., 2013. *Analyst* 138 (4), 1000–1003.
- van Belkum, A., Burnham, C.-A.D., Rossen, J.W.A., Mallard, F., Rochas, O., Dunne, W.M., 2020. *Nat. Rev. Microbiol.* 18 (5), 299–311.
- Wang, K., Li, S., Petersen, M., Wang, S., Lu, X., 2018. *Nanomaterials* 8 (10), 762.
- Yi, Q., Cai, D., Xiao, M., Nie, M., Cui, Q., Cheng, J., Li, C., Feng, J., Urban, G., Xu, Y.-C., Lan, Y., Du, W., 2019. *Biosens. Bioelectron.* 135, 200–207.